Revista Publicando, 5 No 16. (2). 2018, 63-88. ISSN 1390-9304

Petrology of Sirdan volcanic rocks in Alborz Mountains, northern Iran

Fatemeh Ghotb-Tahriri [1], Mohammad-Ali Arian [1*], Shahrooz Haghnazar [2], Mohsen Pourkermani [1]

1- **Department of geology, faculty of science, North Tehran Branch, Islamic Azad University, Tehran, Iran, f.ghotbtahriri@gmail.com, m_arian@iau-tnb.ac.ir, mohsen.pourkermani@gmail .com**
2- **Department of geology, faculty of science, Lahijan Branch, Islamic Azad University, Lahijan, Iran, Haghnazar@liau.ac.ir,**

ABSTRACT

The study area is located around Sirdan town in Sofla-Tarum Mountains in Alborz, south west of Manjil City and west of Loshan, northern Iran. Talesh-Western Alborz volcanic belt was formed by the subduction of Neotethys ocean toward north. However, some researchers believe that the continental rift is responsible for its formation. Firstly, geological field trip was carried out and lithogeochemical samples were collected and prepared for chemical and mineralogical studies. Genetic pattern of the samples was also introduced based on the geochemical analysis and microscopic studies. Sirdan volcanic rocks (northern Iran) include pyroclastic and lava units. Lavas are basalt, andesite, trachyandesite, dacite and riolite. Pyroclastic rocks also consist of different kind of tuffs (lattice crystal tuff, halo lattice tuff, sandy tuff, clay tuff and tuffit), ignimbrite and breccia. Age of the formations belongs to tertiary (mostly Eocene to Oligocene). Basic lavas include olivine, clinopyroxene, plagioclase phenocrysts as well as opaque minerals and plagioclase and clinopyroxene microlite. The dominated texture of the samples is porphyritic microlite. Medium-silica lavas have plagioclase-pyroxene, alkali feldspar, and biotite and amphibole phenocrysts. They also have silica and feldspar microlite and the dominated texture is halo porphyritic. Acidic lavas consist of plagioclase, quartz and alkali feldspar phenocrysts with xenocryst of quartz, feldspar and silica with a dominated texture of porphyry with micro-granular and hyaline. Based on the geochemical analysis, the studied rocks are sub alkaline and tholeiitic. Pattern of rare earth elements shows a high contamination of magma with crustal surface. Finally, the tectonic situation of the studied samples have been introduced from mantle with a source of MORB toward the active marginal continental rift.

Keywords: Sirdan, Iran, Neotethys, crustal contamination, continental active margins

Received 19/08/2018
Approved 02/09/2018

Revista Publicando, 5 No 16. (2). 2018, 63-88. ISSN 1390-9304

1. INTRODUCTION

The studied area is located around Sirdan, southwest of Manjil and west of Loshan, northern Iran. It is located between longitude of 49º00' to 49º15' and latitude of of 36º30' to 36º45' in the southern part of 1:100k geological map of Rudbar. It belongs to Qazvin province. Figs. 1(a) and (b) show satellite images of the area (Google Earth., 2016). The access road is presented by Fig. 2 (Yousefi-Ilani, Alireza., 2004). Based on Iran geological zonation classification (Nabavi, 1976), this area belongs to Alborz- Azarbaijan zone (Fig. 2). According to 1:100K geological map of Rudbar (Nazari, and Salamati, 1998), the dominated outcrops of the region are volcanic and pyroclastic rocks which belong to tertiary (especially Eocene and Oligocene).

Most parts of Iran except Zagros and Kopeh-Dagh had an intensive volcanic plutonic dynamic activities within tertiary which it reached to the highest rate of volcanism and plutonism in Eocene and oligo-Miocene, respectively (Moein-Vaziri, 1996). Cenozoic volcanic rocks have extended in three regions of Alborz, Central Iran and Lut in Iran. (Emami, 2000) believes that the magmatism in tertiary had various lithology types from acidic to basic. From geochemical point of view they have also alkaline to calk-alkaline trends. However, some volcanos have shoshonitic to tholeiitic properties. Generally, there is no common points on the tertiary magmatism of Iran. Some researchers believe that the source of magmatism is Neotethys subduction (in tertiary) and collision of Iran and Arabia blocks. (Berberian and King, 1981; Moein-Vaziri, 1996). Cenozoic magmatism in western Alborz have happened as a result of back oceanic surface subduction of Orumieh Dokhtar and Alborz zone (Alavi, 1996). Talesh- western Alborz volcanic belt was made by the subduction of Neotethys oceanic surface toward north (Innocenti et al., 1982). However, some other researchers believe that the continental rift would play a part. (Didon and Gemain, 1976; Lescuyer and Riou 1976; Emami, 1981). In this paper, the lithological and geochemical properties of the volcanic rocks of Sirdan region (as a part of tertiary magmatism of Alborz-Azarbaijan) have been studied and consequently their magmatic evaluation and tectonic setting of the region have been discussed.

Fig. 1. (a) Aerial image of the region (The studied area is shown by a rectangle (Google Earth, 2016) (b) access road to the region (Yousefi-Ilani, 2004) (the studied region is shown by a circle).

Fig. 2. Location of the studied area on Iran tectonic zones map (Nabavi, 1976).

2. GEOLOGY OF THE ARAE

Based on the geological field trips as well as the geological maps of the area, the dominated outcrops are Neogene red gypsum and conglomerate units, volcanic units, pyroclastic units and granitoid units (with the strike of northwest to south east with the age of tertiary to Eocene-Oligocene). These units are presented in the geological maps by the

Received 19/08/2018
Approved 02/09/2018

Revista Publicando, 5 No 16. (2). 2018, 63-88. ISSN 1390-9304

following abbreviations (in order from oldest to youngest): E^{tv}, E^{v}, E^{t}, E^{ta}, E^{t}_2, E^{v}_1, E^{t}_1, G_1 and G_2 . These units consist interlayers of basic lavas, andesite-basalt lavas, trachyandesite, dacite-rhyolite lavas, pyroclastic units (e.g. Tuffs [lithic crystal tuff, crystal tuff, heliolithic crystal tuff, sandy tuff and clay tuff and tuffit]), ignimbrite and breccia. Intrusive units are granitoid and aplite (Fig. 3).

3. PURPOSES OF THE STUDY

This paper aims to achieve following issues:

a. Petrographic studies and determining the exact chemical composition of rock units in the area
b. Geochemical studies as well as studying the magma evaluation
c. Determining the tectonic origin and providing a reliable tectonomagmatic pattern of the volcanism of the area
d. Studying the influence of contamination and fractional crystallization process on the geochemistry matter of the studied igneous rocks in the studied region.

Fig. 3. Geological map of the studied area (Based on the 1:100K geological map of Rudbar) (Nazari and Salamati, 1998).

4. MATERIALS AND METHODS

All the geological maps of the region as well as the topography maps, satellite and aerial images have been collocated and studies prior to start the geological field trip. Then, a hundred of samples were collected form the area to prepare thin sections which have been studied by the polarized microscope. After the petrographic studies, 23 samples were sent to a laboratory for chemical analysis (ICP-OES, ICP-MS). Table 1. shows the locations where the samples were collected. The chemical results have been analyzed by IGPET and GCD-Kit software so that the geo-genetic pattern of the area was determined.

Table 1- Coordination of the collected samples

5. PETROGRAPHIC STUDY

Based on the petrography studies, the following units can be identified:
First group: olivine basalt and basalt; Second group: Andesite basalt and Andesite; Third group: Trachyandesite; Fourth group: Dacite and rhyodacite; Fifth group: Rhyolite; Sixth group: Pyroclastic rocks.

First group is the most basic igneous rocks (i.e. olivine basalt and basalt). Their texture are porphyritic with microlite to microporphyritic matrix. Intergranular, porphyritic hyalomicrolitic, amygdaloidal and trachyte are among the dominant matrixes in this group.

Received 19/08/2018
Approved 02/09/2018

Revista Publicando, 5 No 16. (2). 2018, 63-88. ISSN 1390-9304

Phenocrysts include olivine, clinopyroxene (augite), plagioclase and opaque minerals. Olivine is gradually eliminated and clinopyroxene gradually increases from olivine-basalt to basalt. Matrix has plagioclase and clinopyroxene (Figs. 4a and b).

Second group include the more fractioned lavas like andesite basalt, andesite, and pyroxene andesite. The textures include hyalo-porphyritic with porphyritic, microlitic, microlitic porphyry, hyalomicrolitic porphyritic and glomeroporphyritic matrix. Phenocrysts are plagioclase, clinopyroxene (augite), orthopyroxene, biotite, amphibole, opaque minerals and some parts of minerals replaced in a secondary process as zeolite. Matrix also consists of dark glass which is mostly prose. Microphenocrysts of plagioclase, pyroxene, biotite and opaque minerals can be seen (Figs. 4c, d and e).

Third group includes trachyandesite and quartz trachyandesite. Their textures are hyalo-porphyritic with glassy, microlitic, microlitic porphyritic, and trachytic matrix. Phenocrysts are plagioclase, alkali feldspar (orthoclase and sanidine), pyroxene (augite), biotite, amphibole, epidote, quartz, and opaque minerals. Matrix includes dark prose glassy microlite with feldspar. It also consists of micro phenocrysts like quartz, feldspar, pyroxene, epidote and opaque minerals (Figure 4f and g).

Fourth group consists of dacite and rhyodacite. They mostly have outcrops around Kallaj and Sirdan villages. The texture is porphyritic with micro-granular matrix. Phenocrysts are plagioclase, alkali feldspar (orthoclase and sanidine), quartz, biotite and opaque minerals. Matrix consist of glass, alkali feldspar, and plagioclase. Plagioclase phenocrysts are shaped to semi-shaped around 1.5 to 2 mm. Plagioclase has zoning and poly synthetic twining in this section which is eroded in some parts. Plagioclase has been mostly sericitized (in a shape of ethmoid). Alkali feldspar phenocrysts are shaped to semi-shaped (around 1 to 1.5 mm). Alkali feldspar mineral has been altered to clay minerals (Sericite) and kaolinitized. They also have double twining. Biotite is also replaced among the minerals as well. Phenocrysts of quartz are shaped to semi-shaped (mostly accumulative and radial in this section, glomera-porphyry). Phenocrysts of biotite are shaped to semi-shaped with the dimension of 1 to 1.5mm. A margin made by the reaction of quartz and plagioclase around the biotite phenocryst can be detected in this thin section. The phenocrysts of the biotite are sometimes skeletal shape. The secondary minerals are chlorite and malachite (Fig. 4h).

Fifth group includes rhyolite. The texture is porphyritic with microgranular matrix. The phenocrysts are plagioclase, quartz and alkali feldspar. The matrix consists of quartz and alkali feldspar crystals. The phenocrysts of plagioclase are shaped to semi-shaped with the dimensions of 0.5 to 1 mm. They are totally altered and turned out to clay minerals. The phenocrysts of quartz are mostly semi-shaped to shaped crystal. These minerals can be detected either as phenocryst or microphenocryst or in the matrix. Alkali feldspar phenocrysts are shaped to semi-shaped with the dimension of 1 to 1.5 mm which have been altered and turned out clay minerals (sericite). Alkali feldspar matrix has been totally turned out to clay minerals (Figure 4i).

Microscopic studies could successfully determine fractional crystallization process in the samples. The least fractionalized crystal is the olivine lava which is consists of olivine

Received 19/08/2018
Approved 02/09/2018

Revista Publicando, 5 No 16. (2). 2018, 63-88. ISSN 1390-9304

phenocryst. This crystals is fractionalized and formed out of olivine. This process is also responsible to increase the concentration of plagioclase and pyroxene in the andesitic basalt samples. As fractional crystallization develops, the rate of pyroxene to plagioclase crystal decreases and amphibole is formed as soon as the magma gets water. This process is almost seen in the andesitic pyroxene. Another process developed via fractional crystallization is the segregation of pyroxene crystals. It sometimes leads to make some quartz crystals in trachyandesite, dacite and rhyolite.

Fig. 4. Microscopic images of the igneous rocks collected for studied area (a) plagioclase, olivine, microlite plagioclase phenocrysts in the basaltic andesite olivine (XPL, 40x) (b) Pyroxene phenocryst in olivine in basaltic andesite olivine (XPL, 40x) (c) Plagioclase phenocrysts and microphenocrysts in andesite (XPL, 40x) (d) Phenocryst of zoned plagioclase in andesite (XPL, 40x) (e) Pyroxene and biotite phenocryst with glomera-porphyry in andesite pyroxene, Pyroxene phenocrysts are detected with skeletal texture; biotite phenocrysts are obvious with sandy-clock twining (XPL, 200x) (f) Phenocrysts of pyroxene, biotite and plagioclase in a matrix of glass, pyroxene phenocrysts with skeletal texture with twining in trachyandesite (XPL, 200x) (g) alkali feldspar and zircon phenocrysts (polyclinic shape) in quartz trachyandesite (XPL, 200x) (h) plagioclase phenocrysts and microphenocrysts in a matrix of glass, plagioclase and alkali feldspar in dacite (XPL, 40x) (i) plagioclase phenocrysts and altered alkali feldspar in a matrix of quartz and alkali feldspar microphenocrysts in rhyolite (XPL, 40x).

6. GEOCHEMISTERY

According to the chemical analysis, the concentration of SiO_2 fluctuates from 45 to 73 percent (Tables 1 and 2). Based on SiO_2 content, three types of rocks can be classified (Basic rocks: SiO_2 45 to 52 percent; Average silica content: SiO_2 52 to 63 percent; Acidic rocks: SiO_2 more than 63 percent).

Table 2- Geochemical results of major elements analysis (ICP and basic melting method) [An: Andesite, Trcy-An: Trachyandesite, Q: Quartz, O1: Olivine]

Table 3- Geochemical results of REEs analysis (with ICP method) [An: Andesite; Trch-An: Trachyandesite; Ba: Basalt; Q: Quartz; O1: Olivine; Pyx: Pyroxene]

In the figure of Total alkaline versus SiO_2 (Cox et al., 1979), basic samples have been classified in the basalt domain, average silica samples have been classified in andesite, andesite basalt, and trachyandesite domain and acidic samples have been classified in the dacite and rhyolite domain. Based on the boundaries between alkaline and sub-alkaline series (Miyashiro, 1978), the basalt samples have been lied on the alkaline- sub alkaline boarder. Two samples

Received 19/08/2018
Approved 02/09/2018

Revista Publicando, 5 No 16. (2). 2018, 63-88. ISSN 1390-9304

from average silica samples have been lied on alkaline region and rest of the samples lied on the sub alkaline area (Fig. 5).

The figures of main oxide element changes can successfully reveal the role of crystalline fractional process on the magma evaluation (Fig. 6). A gradual change of elements from basalt to rhyolite can be seen in all the mentioned figures. As fractional crystallization develops, the concentration of Al_2O_3, CaO, Fe_2O_3 and P_2O_5 decreases and Na_2O and K_2O content increases. It can be related to plagioclase and pyroxene fractional crystallization. The increase of K_2O and Na_2O was caused by magma fraction and ascended magma contamination with potassic crust. Multi-element figures of inconsistent elements known as spider diagrams are used for geochemistry studies of the magma formed the rock units of the area which have been composed in the different tectonic regimes (Wilson, 1989).

Figure 5. Tectonic regime of the studied samples on the diagram of total alkaline elements versus silica (Cox et al., 1979). The boarder between alkaline and sub-alkaline samples have been given through (Miyashiro, 1978). [●: Basalt (mafic) rocks; ■: intermediate (silica) igneous rocks; ▲: felsic (acidic) rocks]

Figure 6. Diagrams of major oxide elements versus silica in the studied samples. [●: Basalt (mafic) rocks; ■: intermediate (silica) igneous rocks; ▲: felsic (acidic) rocks]

Fig. 7 shows the average of normalized REEs versus mantle (Sun and McDonough, 1989). Based on this figure, positive anomalies are K, Pb, Cs, Nd, Sr, and U and negative anomalies are Th, Nb, Pr, P, Ti and Eu, also Rb and Ta shows small negative anomalies. Nd, U and Pb concentration is controlled by Alunite, Sphene, Zircon and Apatite. Generally, separation index of Eu for plagioclase is higher in the andesite than the basalt. Positive anomaly of K was caused by alkali feldspar concentration and negative concentration of P was caused by separation of apatite (Wandji et al., 2008). Negative anomalies of P, Nb and Ta and positive anomalies of K can shows that crust might have played a part in the evaluation of magma in these rocks (Taylor and McLennan, 1985). Figure of REE, the average of normalized elements versus chondrite (Sun and McDonough, 1989), shows a concentration of LREE (100 times) versus a concentration of HREE (10 times). Patterns of mafic, intermediate, and felsic elements are parallel. La, Tm and Tb have concentration while Pr and Yb show have depilation (Fig. 8). The concentration of LREE to HREE was caused due to a strict fractional crystallization as well as crustal contamination. Figure 9 shows a pattern of average REEs versus normalized continental crust values (Rudnick and Fountain, 1995) which have been normalized by primary mantle (Sun and McDonough, 1989). As is observed via the mentioned figures, the rock units of the studied area shows the same pattern which continental crust has.

Figure 7. Pattern of the multi-elements for the normalized (by primary mantle (Sun and McDonough, 1989) inconsistent elements in the studied samples. [●: Basalt (mafic) rocks; ■ : intermediate (silica) igneous rocks; ▲: felsic (acidic) rocks]

Received 19/08/2018
Approved 02/09/2018

Revista Publicando, 5 No 16. (2). 2018, 63-88. ISSN 1390-9304

Figure 8. Pattern of normalized REE (by chondrite) (Sun and McDonough, 1989) for the studied samples. [●: Basalt (mafic) rocks; ■: intermediate (silica) igneous rocks; ▲: felsic (acidic) rocks]

Figure 9. A comparative pattern of normalized REEs (by primary mantle (Sun and McDonough, 1989)) average versus continental crust values (Rudnick and Fountain, 1995). [● : Basalt (mafic) rocks; ■: intermediate (silica) igneous rocks; ▲: felsic (acidic) rocks]

7. TECTONIC REGIMS

In the triangular diagram of (Th-Hf/3-Ta), the samples show a linear trend. All the samples, except one basaltic (mafic) sample located in the region B (E-MORB), most of the samples have been located in the region B (volcanic arcs) (Koglin, 2008). The samples significantly follow the trend of magma and continental interaction (Fig. 10). Diagram of Th/Ta versus Yb (Schandle and Gorton, 2002) shows that the samples follow a trend from mantle source of MORB toward continental active margins (Fig. 11).

Figure 10. Tectonic regime of the samples on the diagram of Th-Hf/3-Ta (Koglin, 2008). (BCC is the average of crustal surface). [●: Basalt (mafic) rocks; ■: intermediate (silica) igneous rocks; ▲: felsic (acidic) rocks]

Figure 11. Location of the studied samples on the diagram of Th/Ta versus Yb (Schandle and Gorton, 2002). [●: Basalt (mafic) rocks; ■: intermediate (silica) igneous rocks; ▲: felsic (acidic) rocks]

8. CONCLUSION

Tertiary eruptions was normally responsible for the rock varieties (from mafic and felsic) everywhere and the studied area is not an exception. Volcanic units have been distributed in the several places of the area. These units have been cut by intrusive units (northwest to southeast). Based on the performed studies, igneous rocks of the studied area have been classified to three types (mafic (basalt), intermediate, and felsic (acidic samples)). Based on the petrographical studies, fractional crystallization can be well highlighted from more mafic ones toward the more felsic forms. Based on the geochemical studies, these samples usually have the sub alkaline and tholeiitic origin. They also have been placed on alkaline and calk alkaline series in some petrological diagrams. Diagrams of major oxides also reveal a significant rule of fractional process from mafic samples toward felsic samples in the magmatic evaluation of the studied rocks. Inconsistent REE pattern of the samples has an equilibrium elemental index with the average of continental surface values. A fluctuated pattern of spider diagrams of the rocks has been caused by crustal contamination in the samples. Negative

Received 19/08/2018
Approved 02/09/2018

Revista Publicando, 5 No 16. (2). 2018, 63-88. ISSN 1390-9304

anomalies of Ta, Nb and P and positive anomaly of K can be a reason of crustal interference in the magma evaluation of these rocks. A weak and limited fractional melting, and crustal separation and contamination can be responsible for the concentration of LREE to HREE.

According to the tectonic setting of the samples (based on the related diagrams), the samples have a tectonic trend from MORB source toward continental surface and convergent plates. It shows a crustal contamination of intraplate basalt and separated terms by a continental crust.

REFERENCES

Alavi, M., 1996, Tectonostratigraphic synthesis and structural style of the Alborz Mountain system in northern Iran. Geodynamic, 21, 1-33.

Berebrian, M., and King, G.C.P., 1981, Towards a paleogeography and tectonic evolution of Iran. Canadian Jounal of Earth Sciences, 18, 210-265.

Cox, K.G., Bell, J.D., and Pankhurst, R.J., 1979, The interpretation of igneous rocks. George Allen and unwin London, London, 450 p.

Didon, J., Gemain, Y. M., 1976, Le Sabalan, Volcan Plio-quaternair de l'Azerbaidjan oriental (Iran); étude géologique et pétrographique de l'edifice et de son environnement régional. Thése de 3éme Cycle, Univ. Grenoble, 304 p.

Emami, M.H., 1981, Géologie de la région de Qom-Aran(Iran). Contribution á l'étude dynamique et géochimique du volcanisme tértiaire de l'Iran central. Thése d'Etat. Univer. Granoble, France, 489 p.

Emami, M.H., 2000, Magmatism in Iran. Geological Survey of Iran, Tehran, 608 p. (In Persian)

Google Earth., 2016, Satellite images.

Innocenti, F., Manetti, P., Mazzuuoli, R., Pasquare, G., and Villari, L., 1982, Anatolia and north-western Iran. In: Thorpe R.S. (ed.). Wiley, J., and Chichester, S., Andesites, orogenic andesites and related rocks. p. 327-349.

Koglin, N., 2008, Geochemistry and petrogenesis and tectonic setting of ophiolites and mafic-ultramafic complexes in the Northeastern Aegean region: New trace-element isotopic and age constraints. Dissertation zur erlangung des grades doktor den naturwissenschaften, Johannes Gutenberg-Universitat, 173 p.

Lescuyer, J.L., Riou, R., 1976, Geologic de la region de mineh (Azerbaijan) Contribution a l'etude du volcanisme tertiaire de l'Iran. These de 3éme Cycle Grenoble, 233 p.

Miyashiro, A., 1978, Nature of alkaline volcanic rock series. Contributions of Mineralogy and Petrology, 66, 91-104.

Moein-Vaziri, H., 1996, An introduction to the Magmatism in Iran, Tarbiyat Moallem University publication, Iran, Tehran, 440 p.

Nabavi, M.H., 1976, An introduction to the geology of Iran. Geological Survey of Iran, Tehran, 109 p. (in Persian)

Nazari, H. and Salamati, R., 1998, Geological Map of Rudbar sheet (1/100000). Geological Survey of Iran, Tehran, 1 p.

Received 19/08/2018
Approved 02/09/2018

Rudnick, R.L. and Fountain, D.M., 1995, Nature and composition of the continental crust: A lower crustal perspective. Reviews of Geophysics, 33, 267-309.

Schandle, E. S. and Gorton, M. P., 2002, Application of high strength elements to discriminate tectonic setting in VMS environments. Economic Geology, 97, 629-642.

Sun, S.S. and McDonough, W.F., 1989, Chemical and isotopic systematics of oceanic basalts: implications for mantle composition and processes. In: Saunders, A.D. and Norry, M.J., (eds) Magmatism in the oceanic basins. Geological Society London Special Publications, 42, 313-345.

Taylor, S. R. and McLennan, S. M., 1985, The continental crust: it's composition and evolution. Blackwell, Oxford, England, 312 p.

Wandji, P., Seuwui, D.T., Bardintzeff, J.M., Bellon, H., and Platevoet, B., 2008, Rhyolites of the Mbépit massif in The Cameroon volcanic line: an early extrusive volcanic episode of Eocene age. Journal of Mineralogy and Petrology, 94, 271-286.

Wilson, M., 1989, Igneous petrogenesis. a global tectonic approach. Unwin Hyman, London, 466 p.

Yousefi-Ilani, Alireza., 2004, Qazvin city roads network map sheet (1/400000), Iran National Cartographic Center, Tehran, 1 p.

LIST OF TABLES AND FIGURES

Table 1. Coordination of the collected samples

Table 2. Geochemical results of major elements analysis (ICP and basic melting method) [An: Andesite, Trcy-An: Trachyandesite, Q: Quartz, O1: Olivine]

Table 3. Geochemical results of REEs analysis (with ICP method) [An: Andesite; Trch-An: Trachyandesite; Ba: Basalt; Q: Quartz; O1: Olivine; Pyx: Pyroxene]

Fig. 1. (a) Aerial image of the region (The studied area is shown by a rectangle (Google Earth, 2016) (b) access road to the region (Yousefi-Ilani, 2004). (the studied region is shown by a circle)

Fig. 2. Location of the studied area on Iran tectonic zones map (Nabavi, 1976).

Fig. 3. Geological map of the studied area (Based on the 1:100K geological map of Rudbar) (Nazari and Salamati, 1998).

Fig. 4. Microscopic images of the igneous rocks collected for studied area (a) plagioclase, olivine, microlite plagioclase phenocrysts in the basaltic andesite olivine (XPL, 40x) (b) Pyroxene phenocryst in olivine in basaltic andesite olivine (XPL, 40x) (c) Plagioclase phenocrysts and microphenocrysts in andesite (XPL, 40x) (d) Phenocryst of zoned plagioclase in andesite (XPL, 40x) (e) Pyroxene and biotite phenocryst with glomera-porphyry in andesite pyroxene, Pyroxene phenocrysts are detected with skeletal texture; biotite phenocrysts are obvious with sandy-clock twining (XPL, 200x) (f) Phenocrysts of pyroxene, biotite and plagioclase in a matrix of glass, pyroxene phenocrysts with skeletal texture with twining in

Received 19/08/2018
Approved 02/09/2018

Revista Publicando, 5 No 16. (2). 2018, 63-88. ISSN 1390-9304

trachyandesite (XPL, 200x) (g) alkali feldspar and zircon phenocrysts (polyclinic shape) in quartz trachyandesite (XPL, 200x) (h) plagioclase phenocrysts and microphenocrysts in a matrix of glass, plagioclase and alkali feldspar in dacite (XPL, 40x) (i) plagioclase phenocrysts and altered alkali feldspar in a matrix of quartz and alkali feldspar microphenocrysts in rhyolite (XPL, 40x).

Figure 5. Tectonic regime of the studied samples on the diagram of total alkaline elements versus silica (Cox et al., 1979). The boarder between alkaline and sub-alkaline samples have been given through (Miyashiro, 1978). [●: Basalt (mafic) rocks; ■: intermediate (silica) igneous rocks; ▲: felsic (acidic) rocks]

Figure 6. Diagrams of major oxide elements versus silica in the studied samples. [●: Basalt (mafic) rocks; ■: intermediate (silica) igneous rocks; ▲: felsic (acidic) rocks]

Figure 7. Pattern of the multi-elements for the normalized (by primary mantle (Sun and McDonough, 1989) inconsistent elements in the studied samples. [●: Basalt (mafic) rocks; ■ : intermediate (silica) igneous rocks; ▲: felsic (acidic) rocks]

Figure 8. Pattern of normalized REE (by chondrite) (Sun and McDonough, 1989) for the studied samples. [●: Basalt (mafic) rocks; ■: intermediate (silica) igneous rocks; ▲: felsic (acidic) rocks]

Figure 9. A comparative pattern of normalized REEs (by primary mantle (Sun and McDonough, 1989)) average versus continental crust values (Rudnick and Fountain, 1995). [● : Basalt (mafic) rocks; ■: intermediate (silica) igneous rocks; ▲: felsic (acidic) rocks]

Figure 10. Tectonic regime of the samples on the diagram of Th-Hf/3-Ta (Koglin, 2008). (BCC is the average of crustal surface). [●: Basalt (mafic) rocks; ■: intermediate (silica) igneous rocks; ▲: felsic (acidic) rocks]

Figure 11. Location of the studied samples on the diagram of Th/Ta versus Yb (Schandle and Gorton, 2002). [●: Basalt (mafic) rocks; ■: intermediate (silica) igneous rocks; ▲: felsic (acidic) rocks]

TABLES

Table 1. Coordination of the collected samples

Sample#	N	E
SG-6	36˚41′20"	49˚12′50"
SG-9	36˚39′23.9 "	49˚11′50.6"
SG-27	36˚41′55.4 "	49˚12′28.1"

Received 19/08/2018
Approved 02/09/2018

Revista Publicando, 5 No 16. (2). 2018, 63-88. ISSN 1390-9304

SG-32	36˚41′51.7"	49˚12′26.8"
SG-35	36˚41′30.2"	49˚12′3.3"
SG-37	36˚42′8"	49˚12′5.1"
SG-39	36˚42′8.2"	49˚12′3.9"
SG-44	36˚42′9.3"	49˚12′2.6"
SG-48	36˚42′22.5"	49˚12′26.6"
SG-54	36˚38′17.1"	49˚10′26.5"
SG-57	36˚31′53.7"	49˚17′31"
SG-58	36˚31′40"	49˚17′42"
SG-60	36˚31′53.8"	49˚17′30"
SG-62	36˚31′53.8"	49˚17′30.5"
SG-64	36˚31′55.3"	49˚17′30.4"
SG-65	36˚32′30.4"	49˚18′17.5"
SG-68	36˚33′11.9"	49˚19′10.3"
SG-72	36˚34′6.3"	49˚20′28.5"
SG-76	36˚33′57.6"	49˚20′27.2"
SG-83	36˚30′53"	49˚16′42"
SG-85	36˚31′33.7"	49˚4′34"
SG-87	36˚35′4.8 "	49˚21′47.1"
SG-89	36˚35′7.5"	49˚21′46.7"

Received 19/08/2018
Approved 02/09/2018

Revista Publicando, 5 No 16. (2). 2018, 63-88. ISSN 1390-9304

Sample#	**SG-57**	**SG-72**	**SG-85**	**SG-54**	**SG-65**	**SG-89**	**SG-62**	**SG-48**	**SG-76**	**SG-35**	**SG-32**
Sample name	**Ol-Basalt**	**Ol-Basaltic andesite**	**Andesite**	**Trachy andesite**	**Q-Trachy andesite**	**Andesite**	**Trachy andesite**	**Trachy andesite**	**Pyroxen-andesite**	**Q-Trachy andesite**	**Pyroxen-Andesite**
					(Wt%)						
SiO_2	49.33	50.44	52.27	52.83	57.81	59.82	60.58	62.19	62.45	62.63	62.69
Al_2O_3	17.64	15.61	14.68	17.8	16.3	16.66	17.19	15.42	16.09	15.63	15.96
CaO	9.99	8.68	9.53	6.58	2.94	3.48	1.64	5.13	4.35	3.74	4.14
Fe_2O_3	2.77	2.48	2.35	2.54	2.47	2.15	2.25	2.05	2.07	1.96	2.02
FeO	6.48	4.4	4.54	4.61	5.17	2.83	3.15	1.47	2.68	1.85	1.84
K_2O	1.25	2.33	3.14	3.77	1.23	3.14	3.14	2.21	1.6	3.49	1.94
MgO	4.96	2.57	4.38	2.9	2.92	2.62	1.74	1.19	1.85	1.82	1.61
MnO	0.3	0.14	0.21	0.18	0.19	0.09	0.1	0.07	0.12	0.08	0.18
Na_2O	3.14	2.83	2.17	3.61	5.71	2.91	6.47	3.08	4.68	3.6	4.25
P_2O_5	0.22	0.31	0.24	0.31	0.22	0.29	0.17	0.16	0.18	0.14	0.17
TiO_2	1.27	0.98	0.85	1.04	0.97	0.65	0.75	0.55	0.57	0.46	0.52
$Mg^{\#}$	50	40.64	54	42.51	41.37	49.61	37.39	38.6	44.5	47.36	45.05
LOI	1.76	8.62	4.58	3.11	3.45	4.79	2.35	5.99	3.44	3.8	4.21
Total	99.84	99.88	99.9	99.8	99.96	99.75	99.89	99.68	99.82	99.41	99.74

Table 2. Geochemical results of major elements analysis (ICP and basic melting method)
[An: Andesite, Trcy-An: Trachyandesite, Q: Quartz, O1: Olivine]

Received 19/08/2018
Approved 02/09/2018

Revista Publicando, 5 No 16. (2). 2018, 63-88. ISSN 1390-9304

Table 2. continue

Sample#	SG-39	SG-27	SG-37	SG-6	SG-9	SG-83	SG-44	SG-58	SG-64	SG-60	SG-68	SG-87
Sample Name	Trcyan	An	An	An	TrcyAn	TrcyAn	Dacite	Q-Trachyandesite	Q-Trachyandesite	Q-Trachyandesite	Trachyandesite	Rhyolite
						(Wt%)						
SiO_2	63.24	63.36	63.41	63.47	64.73	67.09	67.19	68.89	69.78	70.42	72.5	73.13
Al_2O_3	15.84	15.69	15.73	16.35	16.36	15.2	15.47	15.44	15.22	13.89	13.87	12.95
CaO	4.14	3.97	2.85	4.29	3.48	1.8	3.07	1.3	1.17	1.79	0.85	1.37
Fe_2O_3	2.05	2.01	2.08	2.05	2.01	2.04	1.99	1.93	1.91	1.83	1.85	1.82
FeO	1.89	1.77	1.98	1.72	1.92	0.76	1.92	0.73	0.57	0.036	1.62	1.51
K_2O	2.04	1.63	3.97	3.88	4.01	5.61	4.51	4.08	3.86	5.44	5.19	4.37
MgO	1.55	1.75	2.02	0.68	0.76	0.76	0.49	1.07	0.61	0.48	0.28	0.23
MnO	0.1	0.1	0.13	0.13	0.05	0.09	0.03	0.11	0.09	0.14	0.03	0.02
Na_2O	4.44	4.56	3.54	4.29	3.86	2.53	3.41	4.26	4.98	3.56	3.39	3.79
P_2O_5	0.17	0.17	0.16	0.17	0.14	0.05	0.16	0.08	0.08	0.04	0.04	0.04
TiO_2	0.55	0.51	0.58	0.55	0.51	0.54	0.49	0.43	0.41	0.33	0.35	0.32
$Mg^{\#}$	42.2	46.67	48.54	24.61	26.08	33.3	19.04	43.3	32.6	32.35	24.001	21.36
LOI	3.55	4.1	3.17	2.1	1.81	3.32	0.91	1.51	1.17	1.96	1.55	2.01
Total	99.78	99.82	99.84	99.88	99.86	99.88	99.86	99.92	99.92	99.92	99.86	99.91

Received 19/08/2018
Approved 02/09/2018

Revista Publicando, 5 No 16. (2). 2018, 63-88. ISSN 1390-9304

Table 3. Geochemical results of REEs analysis (with ICP method) [An: Andesite; Trch-An: Trachyandesite; Ba: Basalt; Q:Quartz; O1: Olivine; Pyx: Pyroxene]

Sample#	**SG-57**	**SG-72**	**SG-85**	**SG-54**	**SG-65**	**SG-89**	**SG-62**	**SG-48**	**SG-76**	**SG-35**	**SG-32**	**SG-39**
Sample name	**Ol-Ba**	**Ol-Ba an**	**An**	**Trcy an**	**Q-Trachy and esite**	**An**	**Trcy an**	**Trcy an**	**Pyx-and esite**	**Q-Trachy and esite**	**Pyx-and esite**	**Trcy an**
						(ppm)						
Ba	653	625	567	917	365	1059	983	945	799	851	924	832
Ce	40	51	47	56	45	65	61	54	53	53	63	57
Co	29.5	22.5	22.5	18.5	19.9	7.6	10.3	8.5	10.2	7.4	7.5	7.6
Cr	16	55	97	101	22	7	8	7	12	11	9	11
Cu	100	27	45	60	5	19	4	9	35	33	29	22
Cs	3.5	5.7	1.7	4.6	1.1	4.8	1.3	7.3	6.2	3.8	29.7	10.7
Dy	3.61	3.96	4.06	3.73	3.36	4.01	3.59	3.04	3.1	2.45	3.13	3.22
Er	1.94	2.28	2.34	2.16	1.81	2.3	1.77	1.81	1.8	1.34	1.54	1.69
Eu	1.43	1.3	1.39	1.57	1.23	1.79	1.49	1.24	1.21	1.06	1.24	1.27
Fe	7.51	5.29	5.41	5.94	6.26	3.38	3.73	2.49	2.87	2.63	2.61	2.65
Gd	3.35	3.62	3.71	3.58	3.1	4.15	3.15	3.01	3.22	2.4	3.07	3.15
Hf	1.76	3.32	3.09	1.18	1.89	4.33	1.52	2.13	2.57	1.78	2.47	2.27
K	10965	19230	26685	30959	10626	26022	25821	18421	13745	28617	16168	16619
La	16	23	25	29	20	33	28	30	29	29	33	31

Received 19/08/2018
Approved 02/09/2018

Revista Publicando, 5 No 16. (2). 2018, 63-88. ISSN 1390-9304

Lu	0.23	0.31	0.34	0.28	0.21	0.36	0.2	0.25	0.27	0.22	0.23	0.24
Mn	1841	890	1325	1092	1180	549	623	473	750	489	1096	609
Nb	7.2	11.3	9.6	12.8	6.4	12.8	10.7	10.4	10.9	10.3	11.1	11.1
Nd	14.1	19.1	18.3	19.1	14.9	25.4	20.1	18.7	18.5	15	18.9	19.1
Ni	13	19	25	19	9	<1	<1	1	3	3	2	2
P	1114	1449	1221	1619	1175	1503	908	827	886	730	887	864
Pb	13	5	9	11	15	9	23	4	9	8	9	10
Pr	1.9	3.54	3.2	3.6	2.25	5.36	4.11	3.93	3.77	3.1	4.14	4.03
Rb	24	55	75	97	32	66	66	56	81	81	50	50
Sc	26.9	16.4	27.3	18.8	23.1	7.8	9.8	7.2	8.7	6.5	7.5	7.7
Sm	3.9	4.65	4.65	4.57	3.72	5.55	4.54	4.15	4.11	3.44	4.18	4.23
Sr	554.6	442.1	532.4	635.9	217.4	377	380.3	1331.4	531.5	480.4	741.9	581.3
Ta	0.67	0.93	0.8	0.97	0.62	0.99	0.92	0.82	0.85	0.91	0.96	0.86
Tb	0.65	0.68	0.67	0.63	0.61	0.7	0.58	0.54	0.56	0.45	0.53	0.53
Th	1.1	5.82	5.1	6.18	2.13	8.38	4.45	8.49	7.71	7.99	8.75	8.98
Ti	9104	6153	5966	7405	6980	4719	5203	3599	4028	3140	3644	3818
Tm	0.36	0.41	0.44	0.38	0.34	0.42	0.32	0.34	0.37	0.3	0.33	0.34
U	0.5	1.8	1.7	1.5	0.7	2.3	2.01	1.66	2.6	2.3	2.5	2.5
V	288	166	204	201	113	73	109	70	90	64	71	75
Y	16.9	18.9	22	18.8	14	19.8	15.7	16.2	16	12.8	15.7	16.1
Yb	1.7	2	2.1	1.9	1.6	2.2	1.5	1.7	1.7	1.4	1.5	1.6
Zn	162	80	73	105	107	79	122	43	65	73	72	61

Received 19/08/2018
Approved 02/09/2018

Zr	63	133	121	21	24	172	33	61	82	47	70	64
Eu/Eu*	1.2	0.96	1.02	1.18	1.1	1.14	1.2	1.07	1.01	1.12	1.05	1.06

Table 3. continue

Sample#	**SG-27**	**SG-37**	**SG-6**	**SG-9**	**SG-83**	**SG-44**	**SG-58**	**SG-64**	**SG-60**	**SG-68**	**SG-87**
Sample name	**An**	**An**	**An**	**Trcy An**	**Trcy An**	**Dacite**	**Q-Trachy andesite**	**Q-Trachy andesite**	**Q-Trachy andesite**	**Trcy An**	**Rhyolite**
						(ppm)					
Ba	757	825	786	755	829	864	632	756	480	940	348
Ce	57	54	50	45	52	49	67	67	67	57	67
Co	7.2	8.3	8	8	3.9	5.1	3.1	2	1.4	1.6	<1
Cr	8	10	9	8	8	10	7	7	7	6	6
Cu	16	43	16	8	6	17	6	9	7	15	9
Cs	28.2	3	3.6	3.8	4.3	9.7	4.5	3.4	1.8	3.5	2.3
Dy	3.08	2.82	2.44	2.12	3.32	2.77	3.3	2.99	4.33	3.03	3.36
Er	1.69	1.51	1.41	1.13	2.1	1.41	2	1.85	2.92	1.94	2.19
Eu	1.11	1.1	0.96	0.92	0.98	1.02	1.08	1.06	0.78	0.78	0.66
Fe	2.59	2.71	2.65	2.67	2.07	2.71	1.97	1.82	1.37	1.29	1.25
Gd	3.01	2.77	2.36	2.07	2.87	2.58	3.08	2.83	3.71	2.86	3.5
Hf	2.48	1.85	2.2	1.87	2.13	2.11	3.69	3.41	2.43	3.34	2.57
K	13347	32402	30860	31537	46040	35802	33545	30956	44405	41334	36404
La	33	29	26	25	31	25	40	38	37	32	39
Lu	0.24	0.22	0.21	0.17	0.34	0.19	0.29	0.29	0.43	0.34	0.42
Mn	609	825	834	322	553	207	676	553	839	213	130
Nb	10.5	9.7	11	9.9	20.8	11.4	11.4	11.8	20	15	19.7
Nd	18.7	16.7	14.2	12.9	17.1	16.5	19.3	18.4	22.5	17.3	22.8
Ni	2	3	4	2	1	2	<1	<1	<1	<1	<1
P	838	791	853	736	310	793	453	421	247	260	244

Received 19/08/2018
Approved 02/09/2018

Pb	11	6	19	6	27	14	11	7	39	18	21
Pr	3.88	3.44	2.71	2.45	3.67	3.24	4.43	4.19	5.32	4.02	5.51
Rb	49	97	89	91	129	108	105	90	140	132	113
Sc	7.2	7.8	7.1	5.8	5.8	5.5	5.3	4.8	4.4	3.3	4
Sm	3.89	3.74	3	2.66	3.75	3.37	3.73	3.6	4.6	3.41	4.45
Sr	637	357.8	389.5	470.1	175.8	418	246.7	269.2	120.7	140.7	120.2
Ta	0.91	0.87	0.88	0.83	1.48	0.89	0.94	1.02	1.49	1.34	1.52
Tb	0.51	0.47	0.41	0.36	0.56	0.46	0.53	0.5	0.68	0.47	0.59
Th	8.91	8.64	7.57	6.89	10.88	7.27	11.66	12.29	16.69	14.73	16.39
Ti	3441	3361	3532	3199	3612	3378	2679	2444	2227	2061	1980
Tm	0.35	0.3	0.29	0.26	0.4	0.3	0.38	0.38	0.51	0.39	0.42
U	2.4	2	1.9	1.9	3.1	2.5	3.2	3	4.2	3	3.2
V	65	62	70	69	43	71	38	33	22	21	20
Y	16.3	14.7	13.4	11.4	18.1	13	15.1	14.1	23.8	15.5	18.4
Yb	1.7	1.6	1.5	1.2	2.2	1.4	2	2	2.8	2.1	2.2
Zn	68	62	55	44	150	39	58	37	101	77	132
Zr	74	58	61	49	58	63	105	96	69	117	64
Eu/Eu*	0.99	1.04	1.1	1.1	0.91	1.05	0.97	1.01	0.57	0.76	0.51

FIGURES

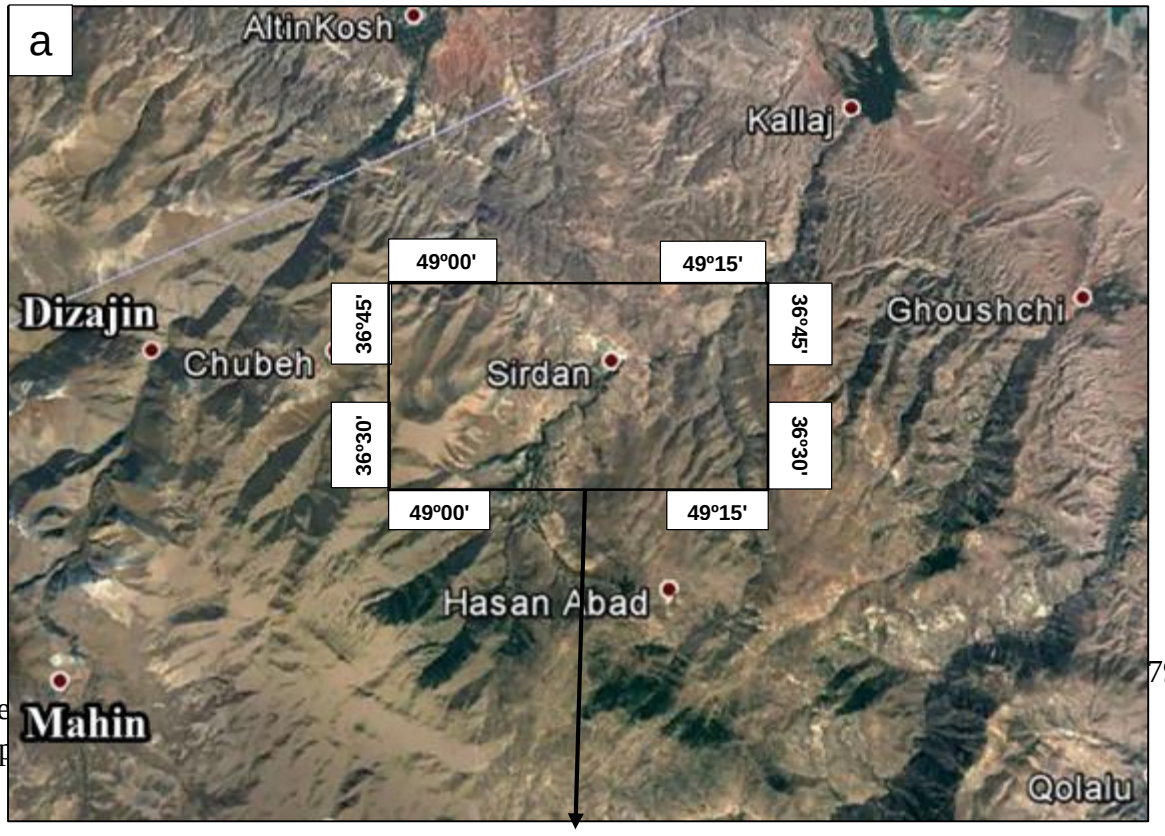

Revista Publicando, 5 No 16. (2). 2018, 63-88. ISSN 1390-9304

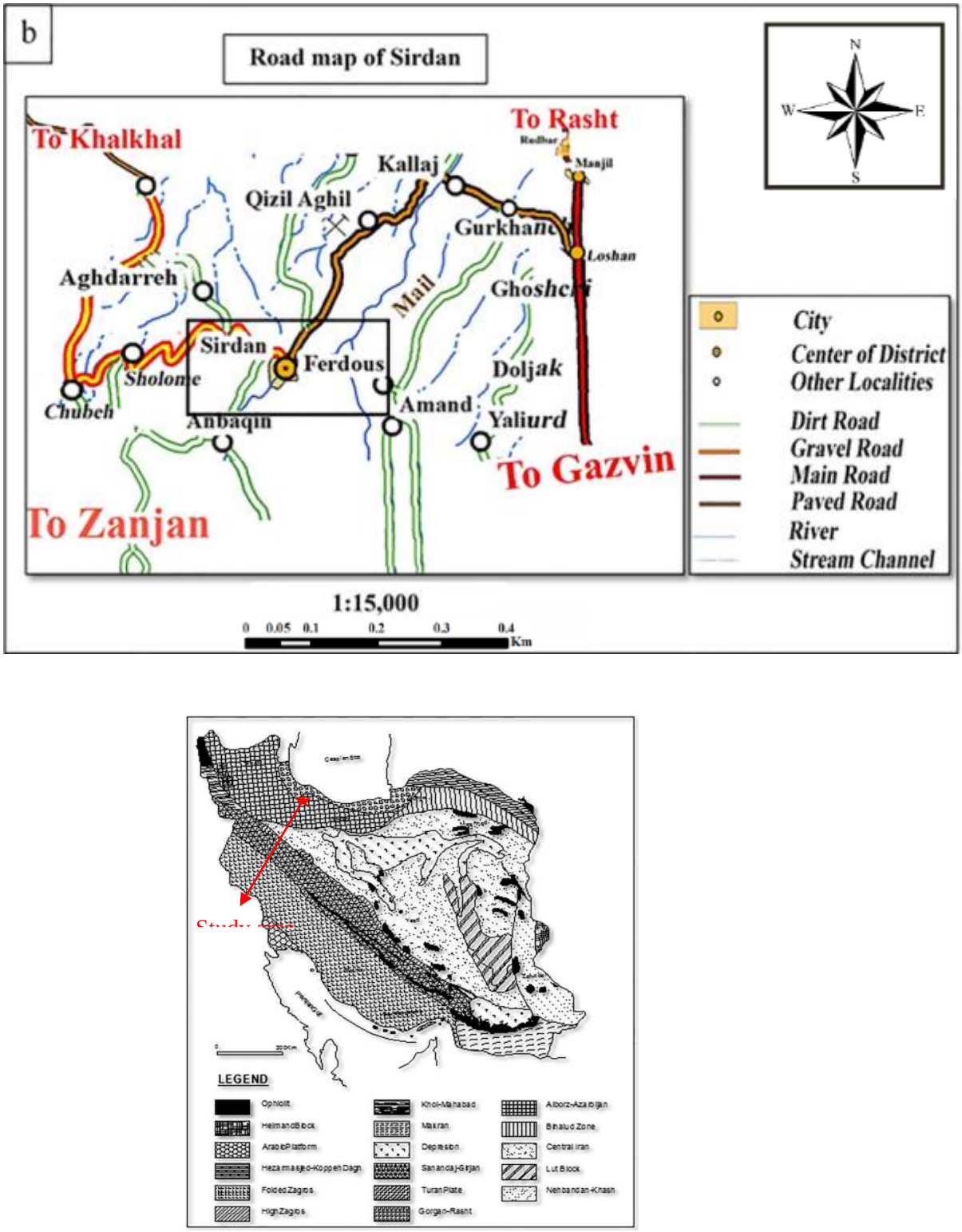

Fig. 2. Location of the studied area on Iran tectonic zones map (Nabavi, 1976).

Received 19/08/2018
Approved 02/09/2018

Revista Publicando, 5 No 16. (2). 2018, 63-88. ISSN 1390-9304

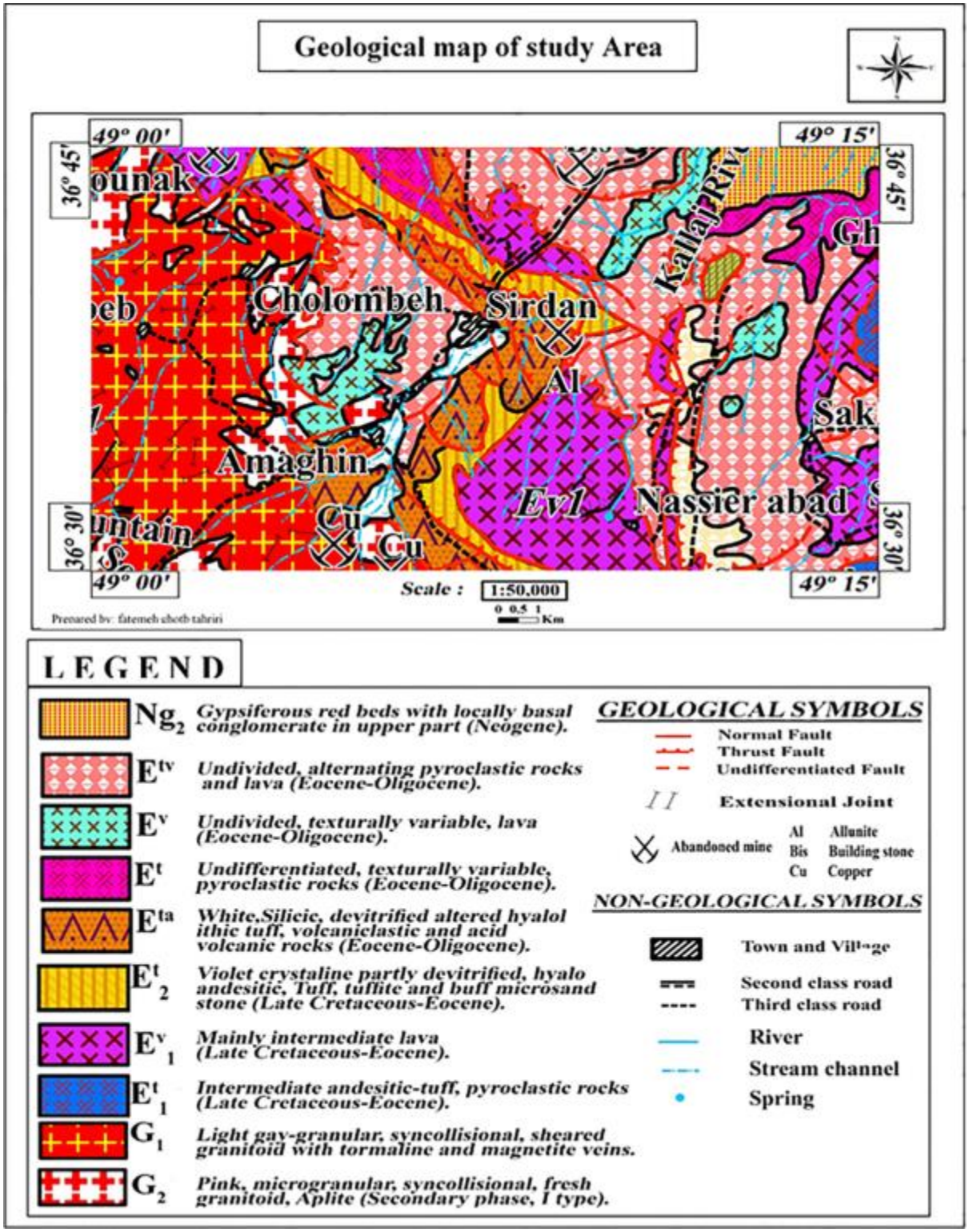

Fig. 3. Geological map of the studied area (Based on the 1:100K geological map of Rudbar) (Nazari and Salamati, 1998).

Received 19/08/2018
Approved 02/09/2018

Revista Publicando, 5 No 16. (2). 2018, 63-88. ISSN 1390-9304

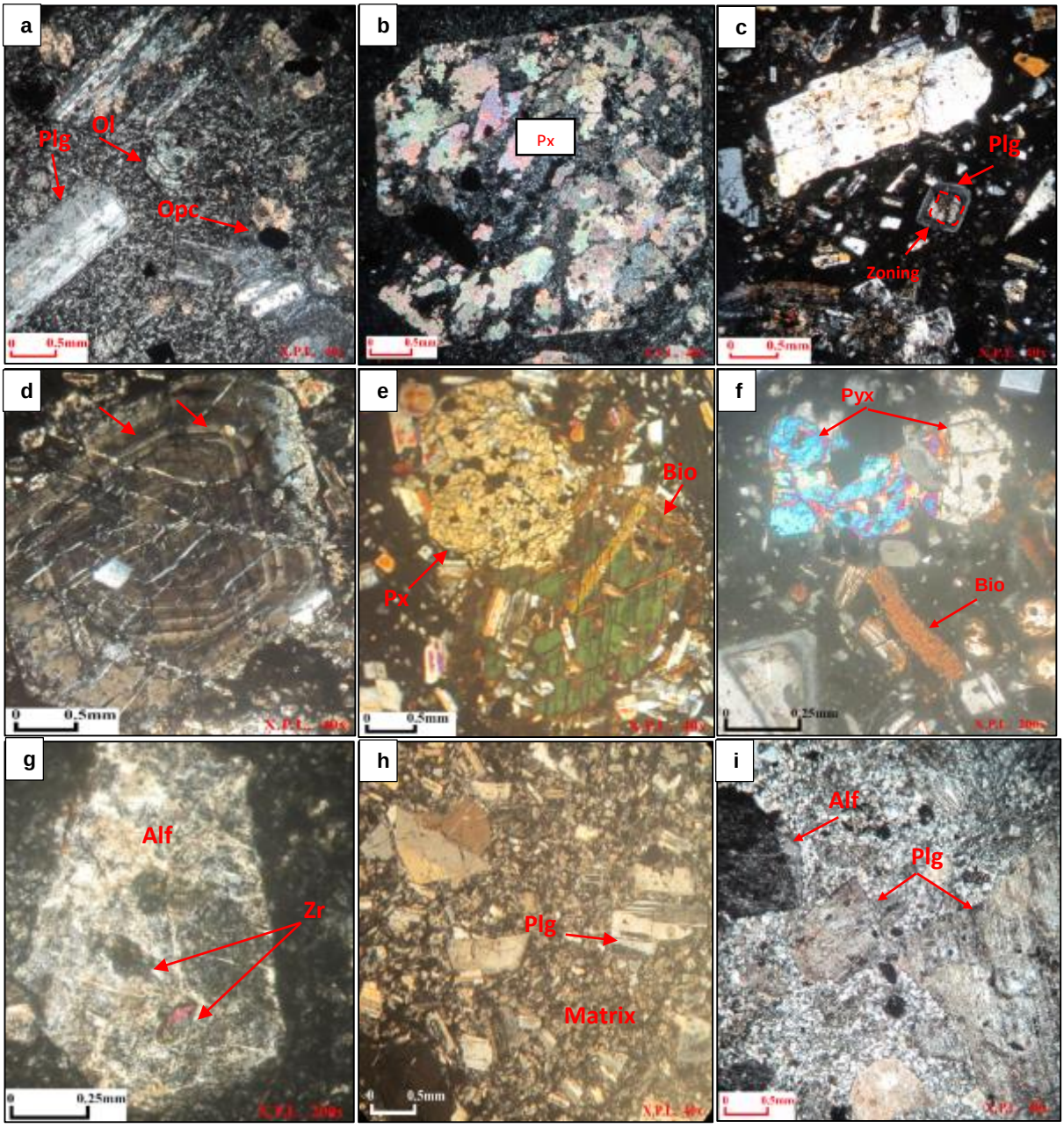

Fig. 4. Microscopic images of the igneous rocks collected for studied area (a) plagioclase, olivine, microlite plagioclase phenocrysts in the basaltic andesite olivine (XPL, 40x) (b) Pyroxene phenocryst in olivine in basaltic andesite olivine (XPL, 40x) (c) Plagioclase

Received 19/08/2018
Approved 02/09/2018

Revista Publicando, 5 No 16. (2). 2018, 63-88. ISSN 1390-9304

phenocrysts and microphenocrysts in andesite (XPL, 40x) (d) Phenocryst of zoned plagioclase in andesite (XPL, 40x) (e) Pyroxene and biotite phenocryst with glomera-porphyry in andesite pyroxene [Pyroxene phenocrysts are detected with skeletal texture; biotite phenocrysts are obvious with sandy-clock twining (XPL, 200x) (f) Phenocrysts of pyroxene, biotite and plagioclase in a matrix of glass [pyroxene phenocrysts with skeletal texture with twining in trachyandesite (XPL, 200x) (g) alkali feldspar and zircon phenocrysts (polyclinic shape) in quartz trachyandesite (XPL, 200x) (h) plagioclase phenocrysts and microphenocrysts in a matrix of glass, plagioclase and alkali feldspar in dacite (XPL, 40x) (i) plagioclase phenocrysts and altered alkali feldspar in a matrix of quartz and alkali feldspar microphenocrysts in rhyolite (XPL, 40x).

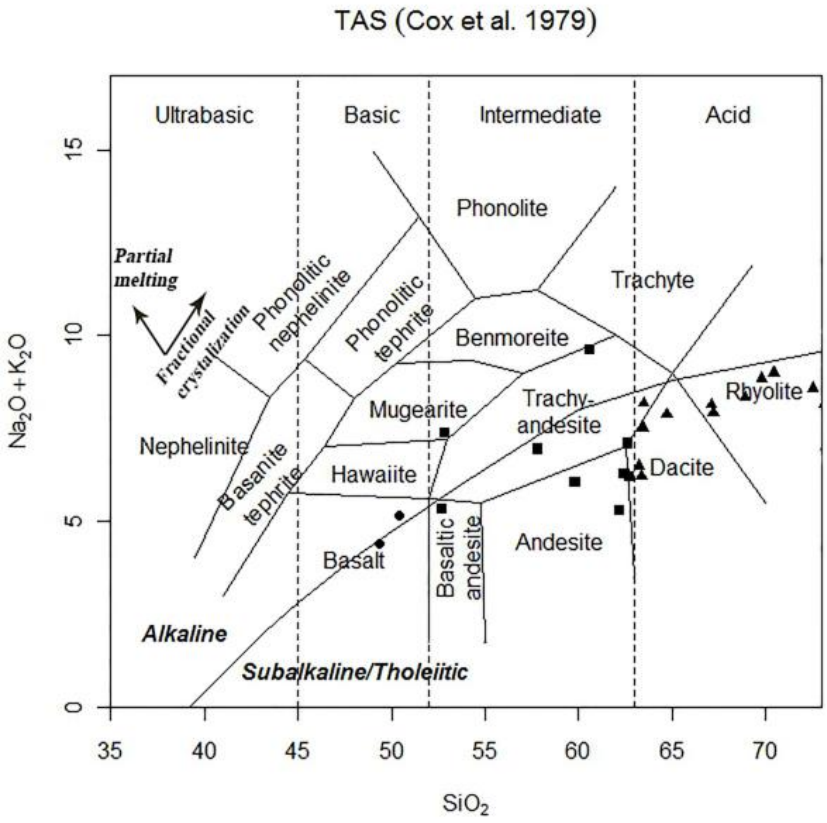

Figure 5. Tectonic regime of the studied samples on the diagram of total alkaline elements versus silica (Cox et al., 1979). The boarder between alkaline and sub-alkaline samples have been given through (Miyashiro, 1978). [●: Basalt (mafic) rocks; ■: intermediate (silica) igneous rocks; ▲: felsic (acidic) rocks]

Received 19/08/2018
Approved 02/09/2018

Revista Publicando, 5 No 16. (2). 2018, 63-88. ISSN 1390-9304

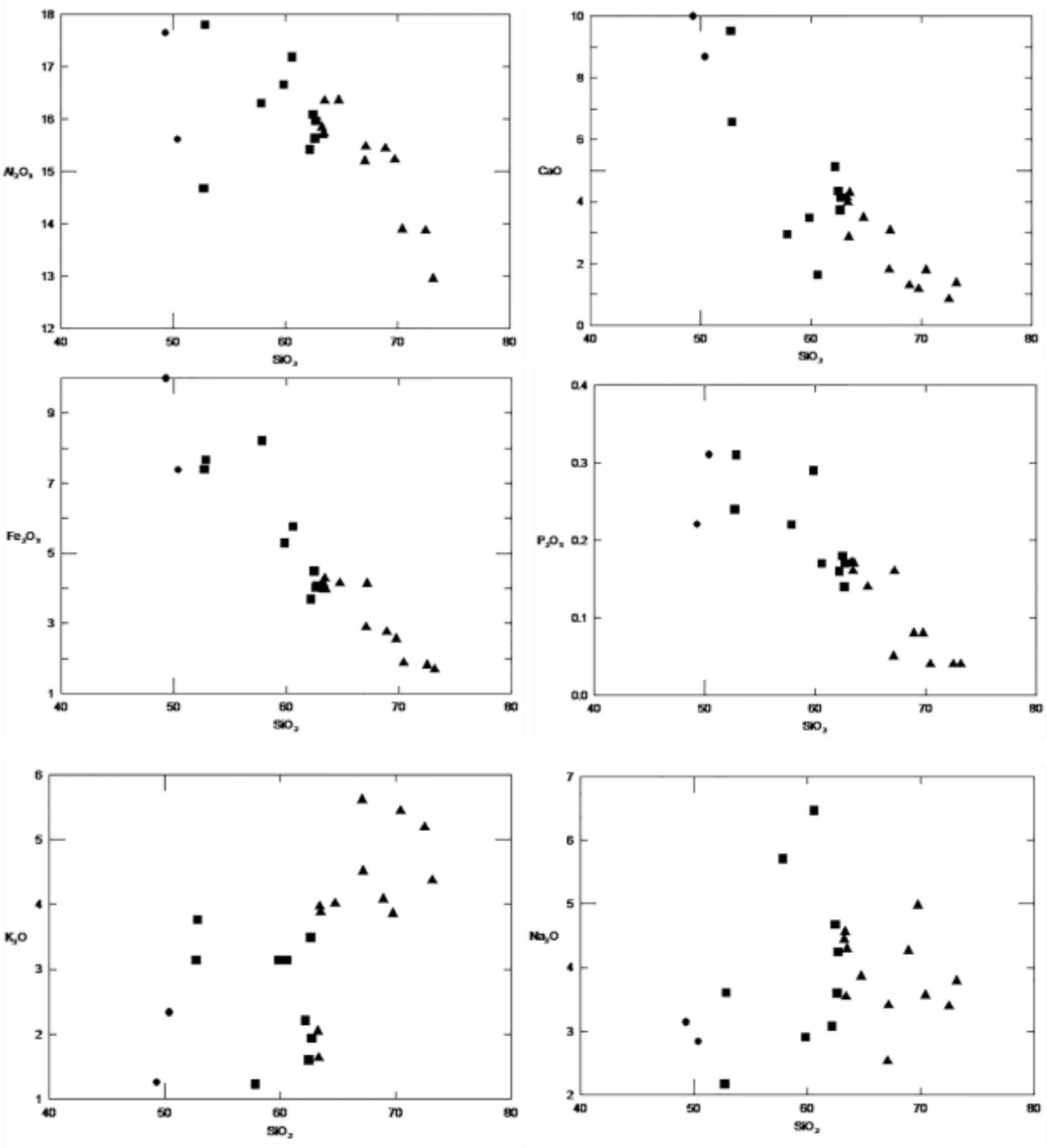

Figure 6. Diagrams of major oxide elements versus silica in the studied samples. [●: Basalt (mafic) rocks; ■: intermediate (silica) igneous rocks; ▲: felsic (acidic) rocks]

Received 19/08/2018
Approved 02/09/2018

Revista Publicando, 5 No 16. (2). 2018, 63-88. ISSN 1390-9304

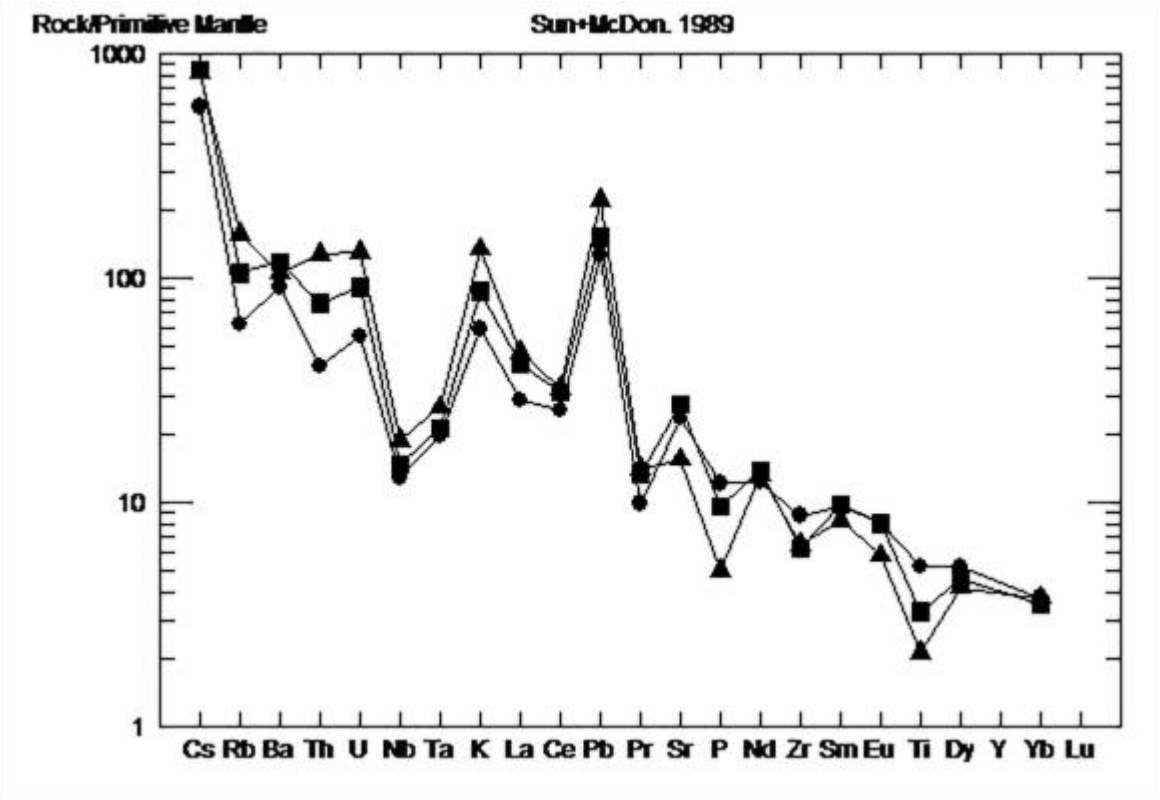

Figure 7. Pattern of the multi-elements for the normalized (by primary mantle (Sun and McDonough, 1989) inconsistent elements in the studied samples. [●: Basalt (mafic) rocks; ■ : intermediate (silica) igneous rocks; ▲: felsic (acidic) rocks]

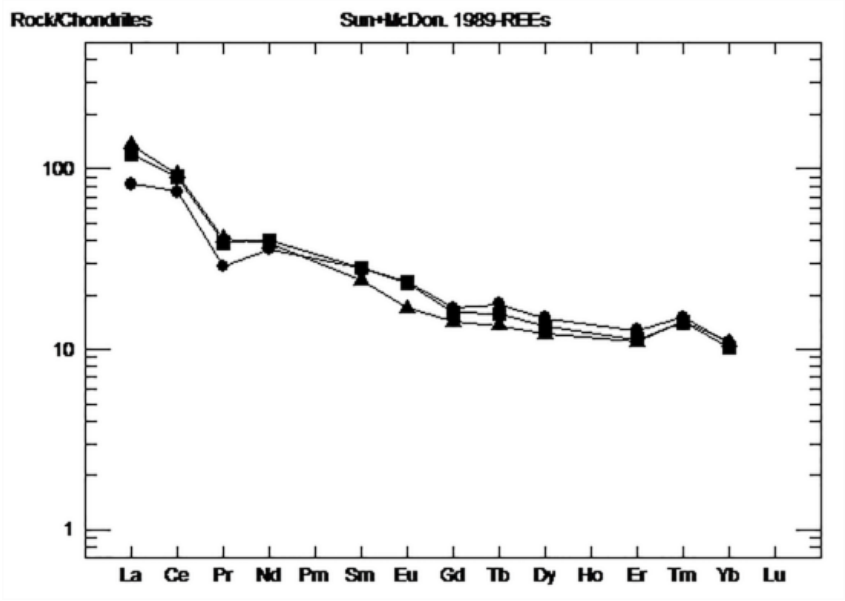

Figure 8. Pattern of normalized REE (by chondrite) (Sun and McDonough, 1989) for the studied samples. [●: Basalt (mafic) rocks; ■: intermediate (silica) igneous rocks; ▲: felsic (acidic) rocks]

Received 19/08/2018
Approved 02/09/2018

Revista Publicando, 5 No 16. (2). 2018, 63-88. ISSN 1390-9304

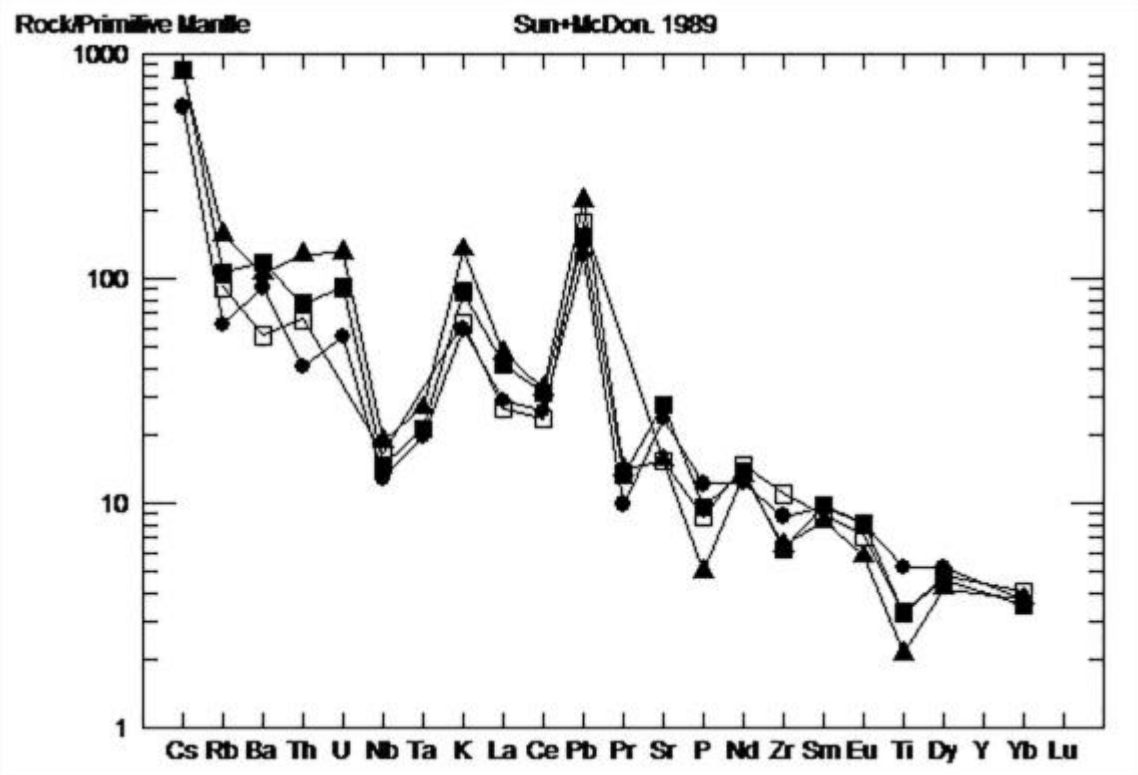

Figure 9. A comparative pattern of normalized REEs (by primary mantle (Sun and McDonough, 1989)) average versus continental crust values (Rudnick and Fountain, 1995). [● : Basalt (mafic) rocks; ■: intermediate (silica) igneous rocks; ▲: felsic (acidic) rocks]

Received 19/08/2018
Approved 02/09/2018

Revista Publicando, 5 No 16. (2). 2018, 63-88. ISSN 1390-9304

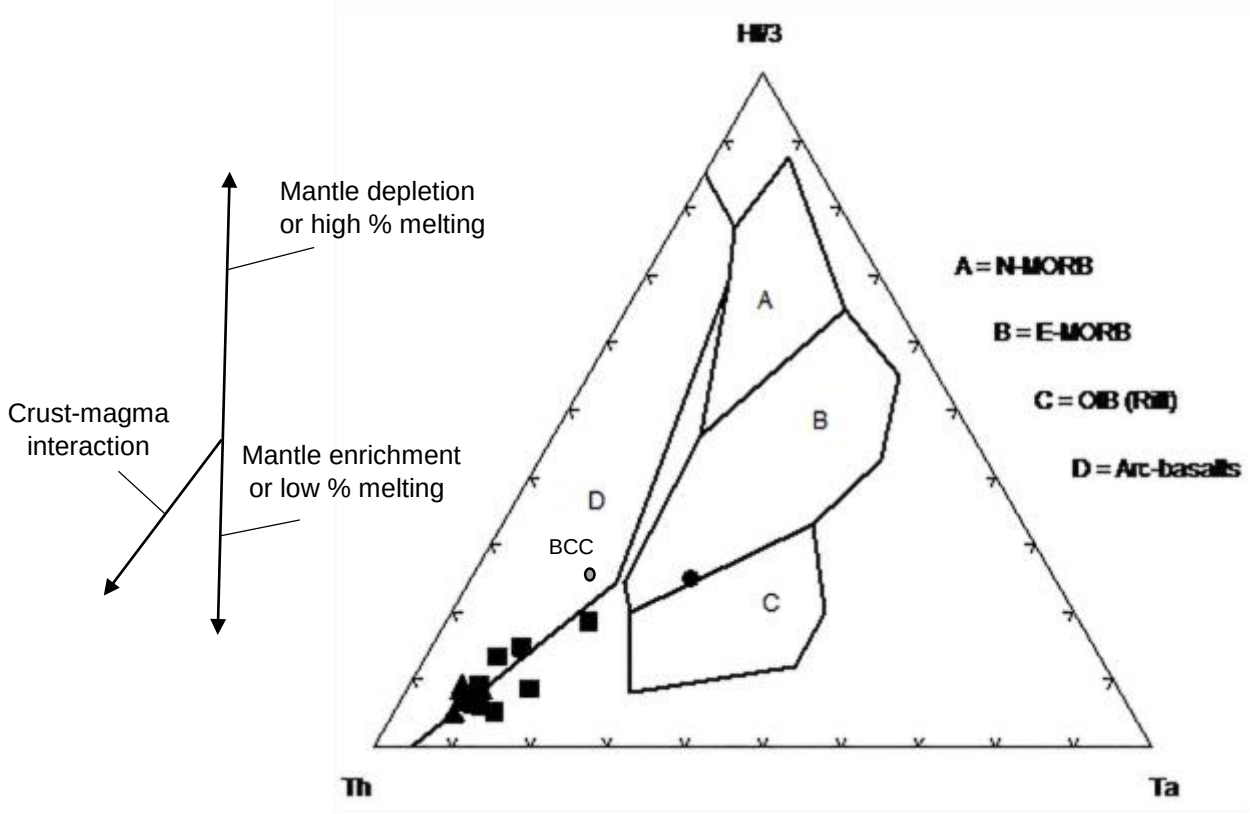

Figure 10. Tectonic regime of the samples on the diagram of Th-Hf/3-Ta (Koglin, 2008). (BCC is the average of crustal surface) (●: Basalt (mafic) rocks; ■: intermediate (silica) igneous rocks; ▲: felsic (acidic) rocks).

Received 19/08/2018
Approved 02/09/2018

Revista Publicando, 5 No 16. (2). 2018, 63-88. ISSN 1390-9304

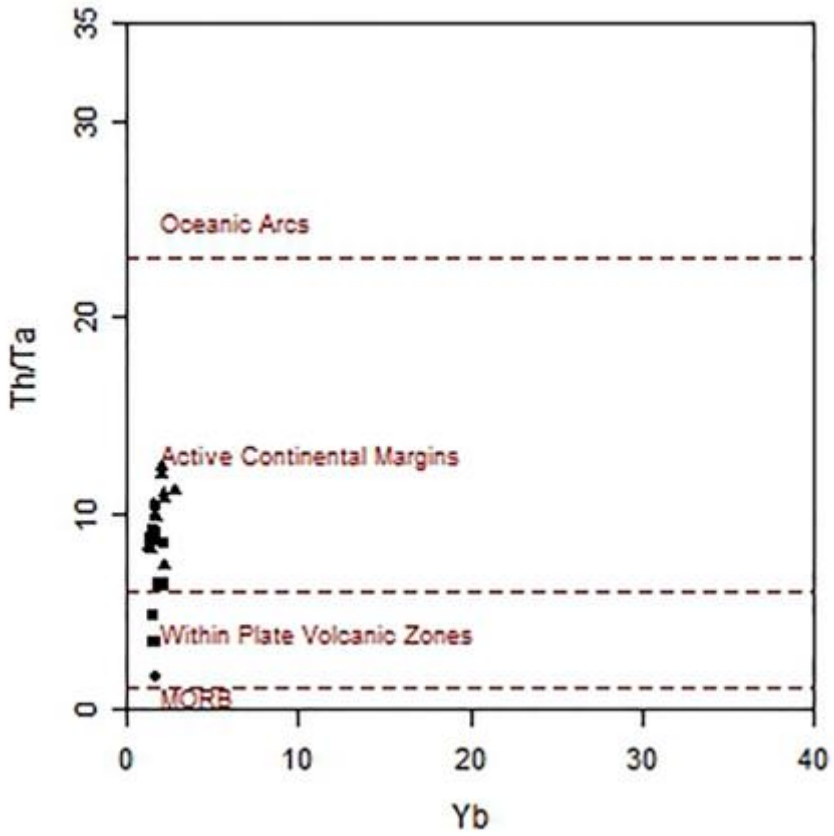

Figure 11. Location of the studied samples on the diagram of Th/Ta versus Yb (Schandle and Gorton, 2002) (●: Basalt (mafic) rocks; ■: intermediate (silica) igneous rocks; ▲: felsic (acidic) rocks).

Received 19/08/2018
Approved 02/09/2018